Progress In Electromagnetics Research B, Vol. 38, 189–203, 2012

ELECTROMAGNETIC INTERFERENCE IMPACT ON FRONT-END RECEIVERS OUTSIDE THE ANTENNA BANDWIDTH

F. Caudron[1, *], A. Ouslimani[1], R. Vézinet[2], and A. Kasbari[1]

[1]Electronic and Control of Systems Lab., EA3649, ENSEA, 6 avenue du Ponceau, Cergy Cedex 95014, France

[2]CEA, DAM, GRAMAT, Gramat F-46500, France

Abstract—Impact of electromagnetic interference on front-end receiver behaviour is theoretically and experimentally studied outside the bandwidth of the antennas. Microwave chaotic generation is observed. Under certain conditions, reflected waves combined to the non linearity of the front-end receiver leads to a chaotic signal generation between the antenna and the front-end receiver. Different antennas, such as patch, loop, monopole and horn, are tested. Theoretical and experimental results are presented for each antenna.

1. INTRODUCTION

When an intentional or an unintentional electromagnetic interference is applied outside of the bandwidth of an antenna, reflection waves are generated between the antenna radiation impedance which is in the case of a few ohms and the nonlinear impedance of the front-end circuit of the receiver which is interconnected to the antenna via a transmission line. Under certain conditions, the effects of the reflected waves due to antenna mismatch combined to those of the nonlinear impedance of the front-end circuits lead to chaos generation. This can have an impact on the electrical behaviour of the receiver particularly for high speed receiver systems and short electromagnetic interference wave lengths.

The chaotic behaviour has already been observed in a microwave limiter circuit [1], in 'R-L-diode' circuits [2–7] and also in VHF microstrip oscillator [8]. The doubling period has been observed

Received 10 November 2011, Accepted 4 January 2012, Scheduled 20 January 2012

* Corresponding author: François Caudron (francaud@ensea.fr).

in 'line-diode' circuits in the case of partial reflection [7]. A delay nonlinear differential equation has been proposed in [9] to study the possible generation of chaos in the front-end microwave limiter receivers. In this paper, we present theoretical and experimental investigations of chaos generation in the front-end receivers for different types of antenna, 2.45 GHz resonant frequency antennas (patch, monopole and loop antennas) and 8.2–12.4 GHz bandwidth horn antenna. For each antenna, theoretical and experimental bifurcation diagrams derived from delay nonlinear differential equation proposed in [9] are exploited to show the existence of the chaos. To the author knowledge, it is the first work which demonstrates the experimental chaos generation in the front-end receivers.

2. IRRADIATED ANTENNAS OUTSIDE THE BANDWIDTH: THEORETICAL ANALYSIS

The equation proposed in [9] is used (Equation (1)) to study the chaos zones from bifurcation diagrams and the attractors. For each antenna, the impedance Z_g which appears in Equation (1) is replaced by the real part of the antenna radiation impedance.

$$V_D(t)-\Gamma(t-T_d)V_D(t-2T_d)+Z_0\left(\left(1+\tau\frac{d}{dt}\right)I(t)+C_{j0}V_0^{\frac{1}{2}}\frac{d}{dt}\frac{V_D(t)}{(V_0-V_D(t))^{\frac{1}{2}}}\right.$$
$$\left.+\Gamma(t-T_d)\left(\left(1+\tau\frac{d}{dt}\right)I(t-2\,T_d)+C_{j0}V_0^{\frac{1}{2}}\frac{d}{dt}\frac{V_D(t-2\,T_d)}{(V_0-V_D(t-2\,T_d))^{\frac{1}{2}}}\right)\right)$$
$$=2\frac{Z_0}{Z_0+Z_g}\left(1+\frac{V_D(t-2\,T_d)-Z_0I_D(t-2\,T_d)}{V_D(t-2\,T_d)+Z_0\,I_D(t-2\,T_d)}\cos\left(2\pi f 2T_d\right)\right)$$
$$E_g\cos\left(2\pi f(t-T_d)\right) \tag{1}$$

with

$$\Gamma(t)=\frac{Z_g-Z_0}{Z_g+Z_0} \tag{2}$$

Using Equations (1), (2) and the antenna radiation impedances, we plot the theoretical bifurcation diagrams and attractors for each antenna (Part 3).

The bifurcation diagrams present the local maxima number of the voltage $V_D\,(t)$ versus the bifurcation parameters f and E_g [9]. The local maxima number is represented on a color scale which ranges from dark blue (period-1) to dark red (chaos). The attractors are realized using the delayed voltage $V_D(t-0.5\,\text{ns})$ versus $V_D\,(t)$.

2.1. Patch Antenna Impedance

The patch antenna is feeded by a quarter-wavelength transmission line of characteristic impedance Z_M and of length L_M to match the antenna to impedance $Z_0 = 50\,\Omega$. In this case, the input impedance Z_{antenna} can be written:

$$Z_{\text{antenna}} = \frac{Z_{\text{patch}} + jZ_M \tan(kL_M)}{1 + j\frac{Z_{\text{patch}}}{Z_M}\tan(kL_M)} \tag{3}$$

Using the impedance transformation equation of transmission lines, the patch input impedance Z_{patch} can be written:

$$Z_{\text{patch}} = G_{\text{slot}}^{-1} // \frac{G_{\text{slot}}^{-1} + jZ_{0_{\text{patch}}} \tan\left(k(L+2\Delta l)\right)}{1 + j\frac{G_{\text{slot}}^{-1}}{Z_{0_{\text{patch}}}} \tan\left(k(L+2\Delta l)\right)} \tag{4}$$

where L is the length of the patch, $k = 2\pi f\sqrt{\varepsilon_r}c^{-1}$ the wave number, and f and c, respectively, the frequency and the speed of light in vacuum equal to 3 ($10^8\,\text{ms}^{-1}$).

Because of the fringing effects, the electrical dimensions of the patch antenna are greater than its physical ones. The patch antenna dimensions are then extended by a length Δl on each end [11].

$$\Delta l = 0.412h\frac{(\varepsilon_{\text{reff}} + 0.3)\left(\frac{W}{h} + 0.264\right)}{(\varepsilon_{\text{reff}} - 0.258)\left(\frac{W}{h} + 0.8\right)} \tag{5}$$

with W the width of the patch and h the thickness of the dielectric sheet.

For $W/h \gg 1$, the characteristic impedance of the patch $Z_{0_{\text{patch}}}$ is given by [11, 13]:

$$Z_{0_{\text{patch}}} = \frac{120\pi}{\sqrt{\varepsilon_{\text{reff}}}\left(\frac{W}{h} + 1.393 + 0.667\ln\left(\frac{W}{h} + 1.444\right)\right)} \tag{6}$$

where

$$\varepsilon_{\text{reff}} = \frac{\varepsilon_r + 1}{2} + \frac{\varepsilon_r - 1}{2}\left(1 + 12\frac{h}{W}\right)^{-\frac{1}{2}} \tag{7}$$

The patch antenna radiating slot is represented by an equivalent conductance G_{slot} of the antenna [10, 11]:

$$G_{\text{slot}} = G_a + G_m \tag{8}$$

with

$$G_a = \frac{1}{120\pi^2}\int_0^\pi g(\theta)d\theta \tag{9}$$

$$G_m = \frac{1}{120\pi^2}\int_0^\pi g(\theta)J_0\left(k_0 L\sin(\theta)\right)d\theta \tag{10}$$

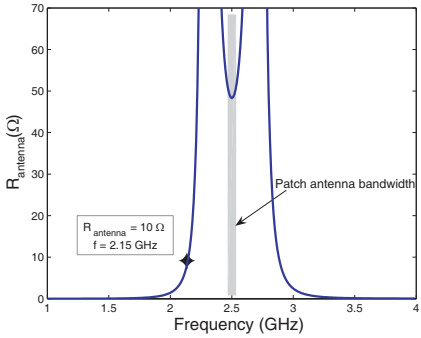

Figure 1. Theoretical R_{antenna} with $L = 3.8\,\text{cm}$, $W = 4.59\,\text{cm}$.

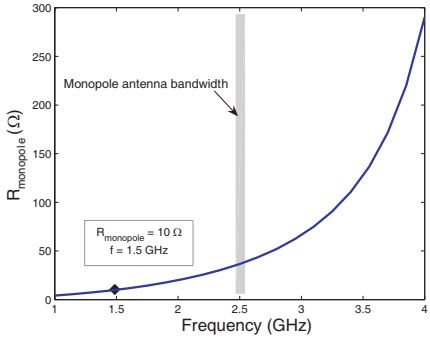

Figure 2. Theoretical R_{monopole} with $l = 3\,\text{cm}$.

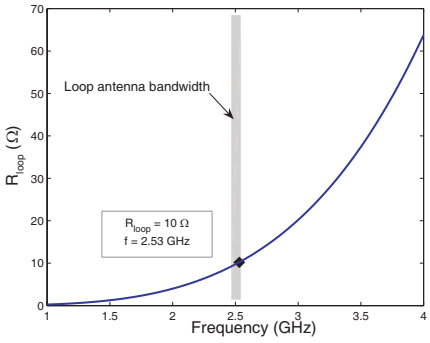

Figure 3. Loop antenna resistance with $2a = 18\,\text{mm}$.

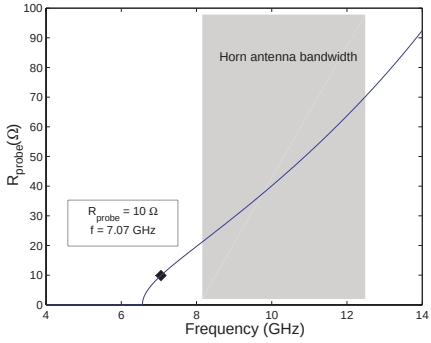

Figure 4. Probe resistance of the horn antenna.

where G_a is the main conductance of the slot and G_m the mutual conductance defined in terms of the far-zone fields. $k_0 = 2\pi f c^{-1}$, J_0 is the Bessel function of the first kind of order zero and $g(\theta)$ defined as:

$$g(\theta) = \left(\frac{\sin\left[\frac{k_0 W}{2}\cos(\theta)\right]}{\cos(\theta)} \right)^2 \sin(\theta)^3 \tag{11}$$

Figure 1 depicts the real part R_{antenna} versus frequency calculated from Z_{antenna}. In [9], we have shown that the chaos appears for $Z_g \leq 10\,\Omega$. For each antenna, the value $R_{\text{antenna}} = 10\,\Omega$ is indicated in Figure 1 to Figure 4.

Using Equations (1)–(3), we plot the theoretical bifurcation diagram with $Z_g = R_{\text{antenna}}$, $T_d = 10\,\text{ns}$ and $Z_0 = 50\,\Omega$ (Figure 7(a),

Part 3).

We observe that the chaos appears from $E_g > 1\,\mathrm{V}$ in the three areas (see Figure 7(a)). One the other hand, the behavior is periodic (period-1) from $f > 2\,\mathrm{GHz}$ and $\forall E_g \in]0, 2]\,\mathrm{V}$.

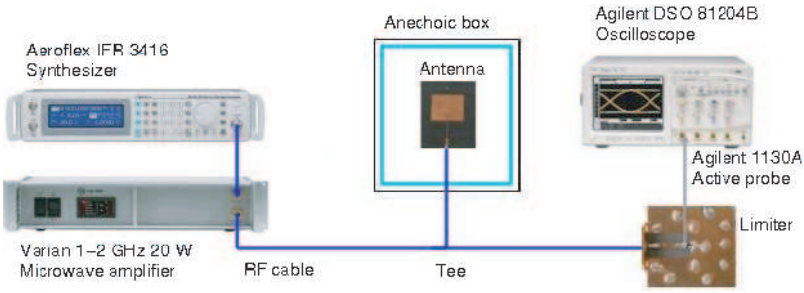

Figure 5. A schematic of measurement setup.

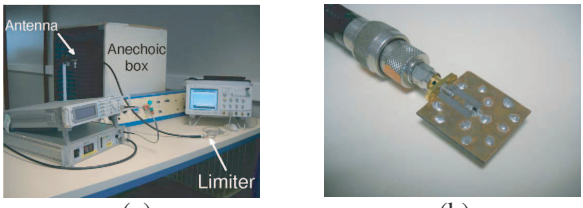

Figure 6. Experiments, (a) measurement setup, (b) front-end RF limiter circuit.

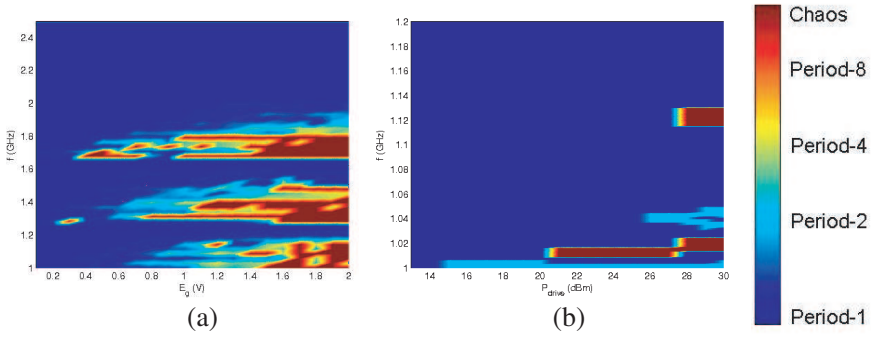

Figure 7. Results with the patch antenna, (a) the theoretical bifurcation diagram from Equations (1)–(3), (b) the experimental bifurcation diagram.

2.2. Monopole antenna impedance.

Equation (12) gives the resistance R_{monopole} of the radiation impedance for a monopole antenna [11]

$$R_{\text{monopole}} = \frac{\eta}{4\pi \sin^2(kl)} \left(C + \ln(2kl) - Ci(2kl) + \frac{1}{2}\sin(2kl)\,(Si(4kl) \right.$$
$$\left. -2Si(2kl)) + \frac{1}{2}\cos(2kl)\,(C + \ln(kl) + Ci(4kl) - 2Ci(2kl)) \right) \qquad (12)$$

where Ci and Si are the cosine and sine integral functions, l the monopole length, a the monopole radius, $k = 2\pi f c^{-1}$ with $c = 3(10^8\,\text{ms}^{-1})$, $\eta = 120\pi\,\Omega$ (impedance in free space), and $C = 0.577$.

Figure 2 depicts the calculated R_{monopole} versus frequency.

The theoretical bifurcation diagram with $Z_g = R_{\text{monopole}}$, $T_d = 10\,\text{ns}$ and $Z_0 = 50\,\Omega$ is plotted (Figure 8(a), Part 3). The chaos appears in the two areas (see Figure 8(a)). The behavior is periodic (period-1 and period-2) $\forall f$ and $E_g \geq 1.3\,\text{V}$.

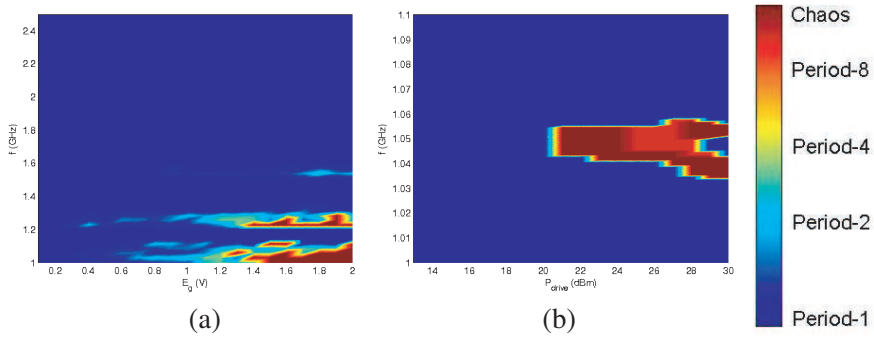

(a) (b)

Figure 8. Results with the monopole antenna, (a) the theoretical bifurcation diagram, (b) the experimental bifurcation diagram.

2.3. Loop antenna impedance.

The radiation resistance for a single-turn loop can be written as [11]:

$$R_{\text{loop}} = 20\pi^2 \left(\frac{C_{\text{irc}}}{\lambda} \right)^4 \qquad (13)$$

where $C_{\text{irc}} = 2\pi a$ is the circumference of the loop antenna, a the loop radius, and $\lambda = c/f$ with $c = 3\,(10^8\,\text{ms}^{-1})$. Figure 3 depicts R_{loop} versus frequency.

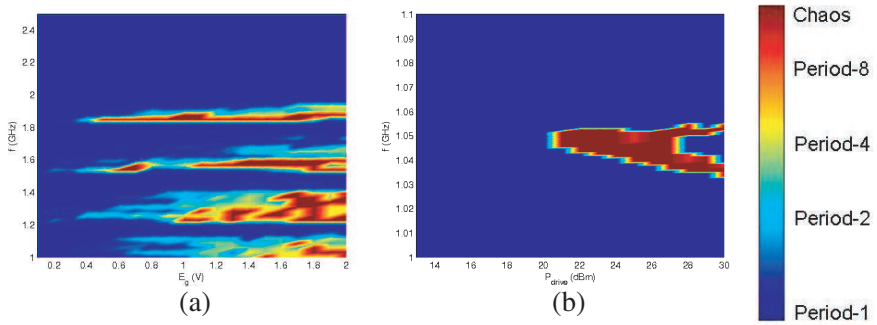

Figure 9. Results with the loop antenna, (a) the theoretical bifurcation diagram, (b) the experimental bifurcation diagram.

Using Equation (13), we plot the theoretical bifurcation diagram with $Z_g = R_{\text{loop}}$, $T_d = 10\,\text{ns}$ and $Z_0 = 50\,\Omega$ (Figure 9(a), Part 3). We observe that the chaos appears in the four areas (see Figure 9(a)).

2.4. Horn Antenna Impedance

This impedance is given by the probe antenna which consists of a waveguide-transmission line transition with its inner conductor extending into the rectangular waveguide. The probe radiation impedance Z_{probe} is given by:

$$Z_{\text{probe}} = \frac{V}{I_0} = \frac{V}{\int_0^{2\pi} J_y(0) r d\phi} \tag{14}$$

Function J_y represents the current density along the probe. Parameter V is the applied voltage at the probe antenna. Expanding the current density J_y in terms of a suitable set of basis functions $\psi_n(y)$ and using the Green's theorem, Equation (14) becomes [12]:

$$Z_{\text{probe}} = \frac{\Sigma_{n=1}^{N} \Sigma_{m=1}^{N} G_{nm} I_n I_m}{\Sigma_{n=1}^{N} I_n \Sigma_{m=1}^{N} f_n I_n} \tag{15}$$

with

$$G_{nm} = -\frac{1}{(2\pi r)^2} \iint_{S_0} \iint_{S_0} \psi_n(y) G_{yy}(r, r') \psi_m(y') dS dS' \tag{16}$$

and

$$f_n = \int_0^d \psi_n(y) e(y) dy \tag{17}$$

The function $e(y)$ is a normalized electric field along the probe. Figure 4 depicts the calculated $R_{\text{probe}} = \text{Re}\{Z_{\text{probe}}\}$ versus frequency.

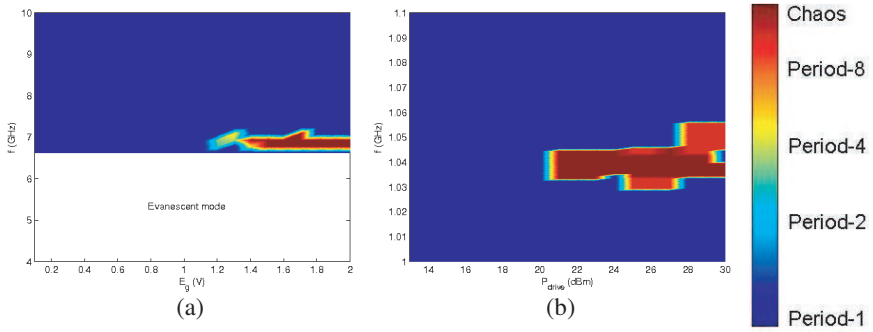

Figure 10. Results with the horn antenna (the horn *Sivers Lab.* PM7320X/01 and the waveguide-transmission line transition HP X281A): (a) the theoretical bifurcation diagram, (b) the experimental bifurcation diagram.

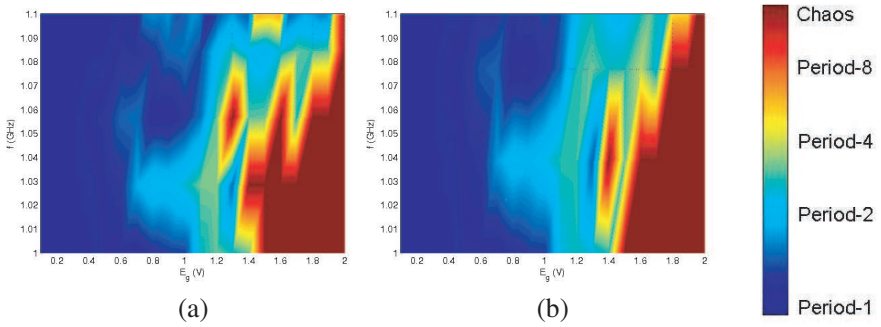

Figure 11. Results with the monopole antenna. (a) The theoretical bifurcation diagram obtained from Equation (1), (b) the bifurcation diagram obtained from the equivalent circuit.

Using Equations (14)–(17), we plot the theoretical bifurcation diagram with $Z_g = R_{\text{probe}}$, $T_d = 10\,\text{ns}$ and $Z_0 = 50\,\Omega$ (Figure 10(a), Part 3). We observe that the chaos appears in the one area (see Figure 10(a)). In the evanescent mode, the impedance R_{probe} is equal to zero. Consequently, there is no power in the front-end receiver circuit.

3. THEORETICAL AND EXPERIMENTAL RESULTS

Figure 5 presents the measurement setup.

The driving source is realized with a synthesizer Aeroflex IFR 3416 8 GHz followed by a power amplifier Varian 1–2 GHz 20 W. The

amplifier output power is rated P_{drive}.

Measurements have been realized with an oscilloscope Agilent DSO 81204B 12 GHz 40 GSa/s and an active probe Agilent 1130A 1.5 GHz. Different type of antennas, horn antenna (2.45 GHz patch antenna), commercial antennas (2.45 GHz monopole and loop antennas [14], 8.2–12.4 GHz horn antenna) are tested. Antennas are placed into an anechoic box (Figure 6(a)). Because of the limits of the measurements setup (power amplifier and active probe), measurements have been made up to 1.5 GHz. The front-end RF limiter circuit is realized with a PIN diode "$BAP64$-02" for applications up to 3 GHz. Figures 7 to 10 depict the theoretical and experimental bifurcation diagrams. The bifurcation parameters are the frequency f and E_g driving voltage for theoretical part, and f and P_{drive} for experimental

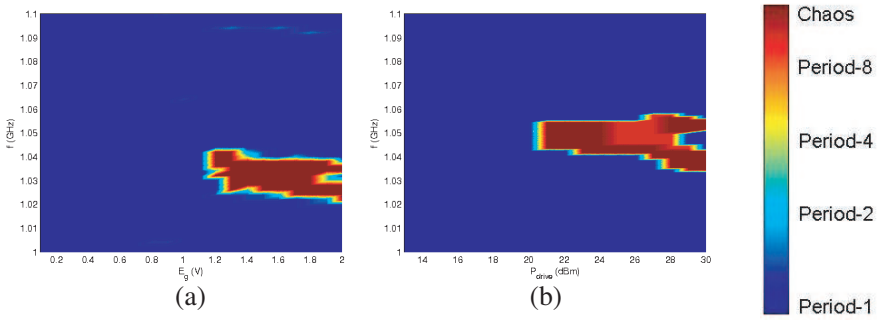

Figure 12. Results with the monopole antenna, (a) the bifurcation diagram obtained from the equivalent circuit with the critical elements, (b) the experimental bifurcation diagram.

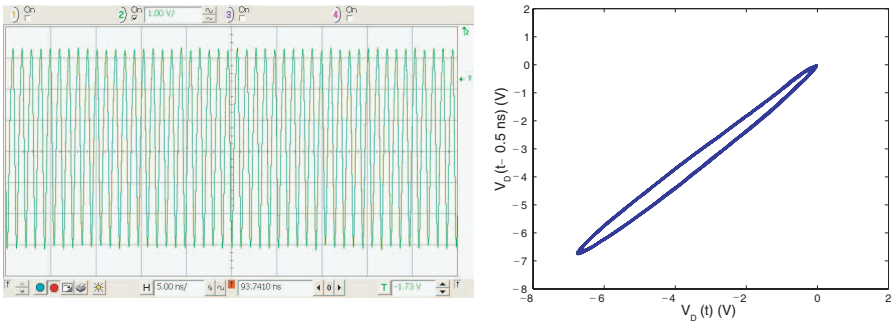

Figure 13. Experimental periodic behaviour for the patch antenna at $f = 1025$ MHz for $P_{\text{drive}} = +24$ dBm. (a) Screenshot showing the voltage $V_D(t)$, (b) experimental attractor.

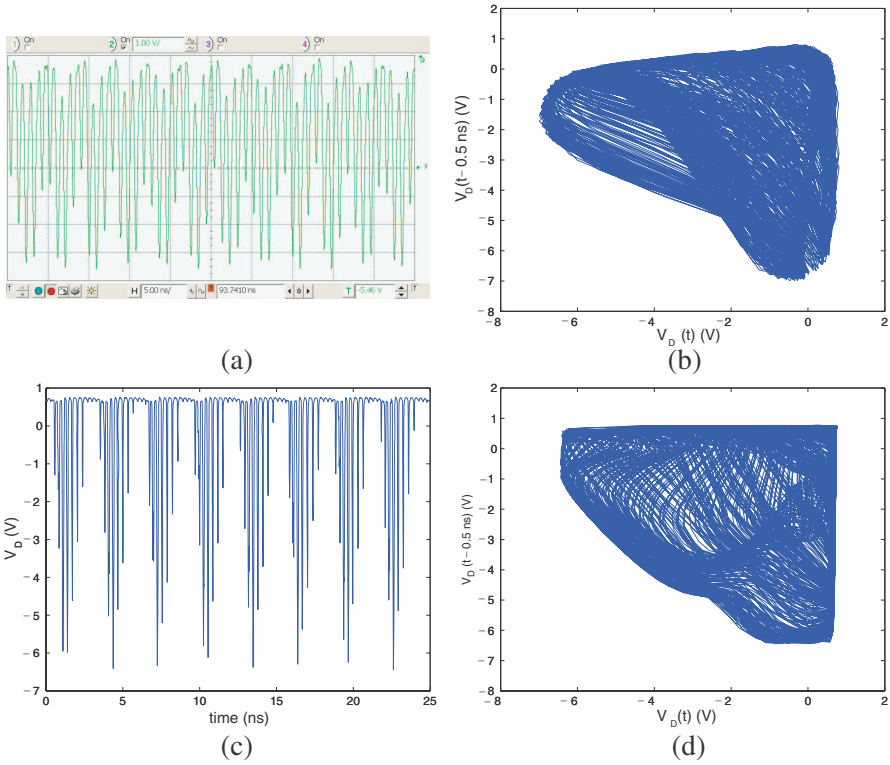

Figure 14. Theoretical and experimental chaotic behaviour for the patch antenna in the chaos conditions Table 1. (a) Screenshot showing the voltage $V_D(t)$, (b) experimental chaotic attractor, (c) theoretical voltage $V_D(t)$ using Matlab, (d) theoretical chaotic attractor using Matlab.

Table 1. Theoretical and experimental chaos conditions.

Antennas	Theoretical chaos conditions			Experimental chaos conditions	
	f (MHz)	E_g (V)	Z_g (Ω)	f (MHz)	P_{drive} (dBm)
Patch	1025	2	0.1	1025	+29
Monopole	1039	2	4.0	1039	+28
Loop	1042	2	0.3	1042	+28
Horn	1040	2	2.0	1040	+28

part. All the results show the chaotic behavior zones (see dark red area). Doubling period, period-4 are also demonstrated.

The experimental zones are narrower than the theoretical chaotic

zones, due to the effect of experimental setup. Indeed, the critical elements, such as coaxial and microstrip lines and the input impedance of the active probe, are not included in the theoretical results deduced from Equation (1) and shown in Figures 7(a) to 10(a). All the antenna measurements use the same test setup, then we choose to study the effect of the critical elements only for the monopole antenna. To account for these critical elements, we have first compared in Figure 11 the theoretical results obtained from Equation (1) and the electrical simulations deduced from an equivalent circuit. The transmission line is described by an ideal line defined only by its characteristic impedance and its delay time.

One can note that the results obtained from the equivalent circuit are not far from those given by the Equation (1).

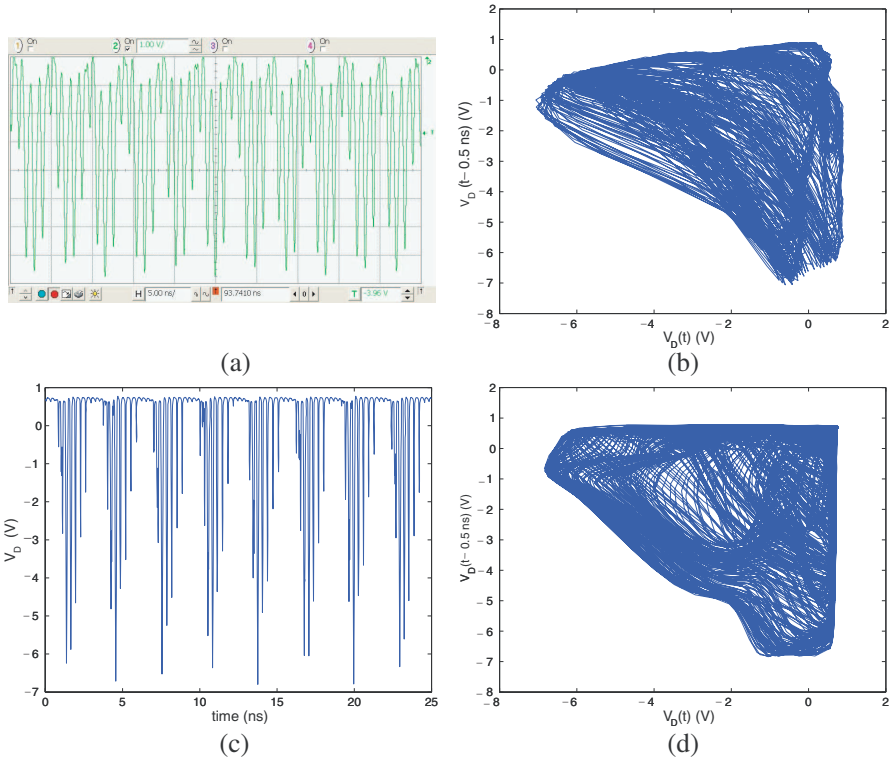

Figure 15. Theoretical and experimental chaotic behaviour for the monopole antenna in the chaos conditions Table 1. (a) screenshot showing the voltage $V_D(t)$, (b) experimental chaotic attractor, (c) theoretical voltage $V_D(t)$ using Matlab, (d) theoretical chaotic attractor using Matlab.

In the second one, each critical element is characterized and added to the previous circuit: the ideal line is described by a coaxial and microstrip line ADS model and the input of the active probe is modeled by its equivalent electrical parameters given by the constructor ($R_{\text{active probe}} = 25\,\text{k}\Omega$ and $C_{\text{active probe}} = 0.67\,\text{pF}$). Experimental results and simulation results which account for the critical elements are presented in Figure 12. The simulation results demonstrate the effect of the critical elements on the chaotic behaviour and we can note that these results are not far from the experimental results.

Because the experimental setup frequency limitation is up to 1.5 GHz, the horn antenna is tested in the area of the evanescent mode

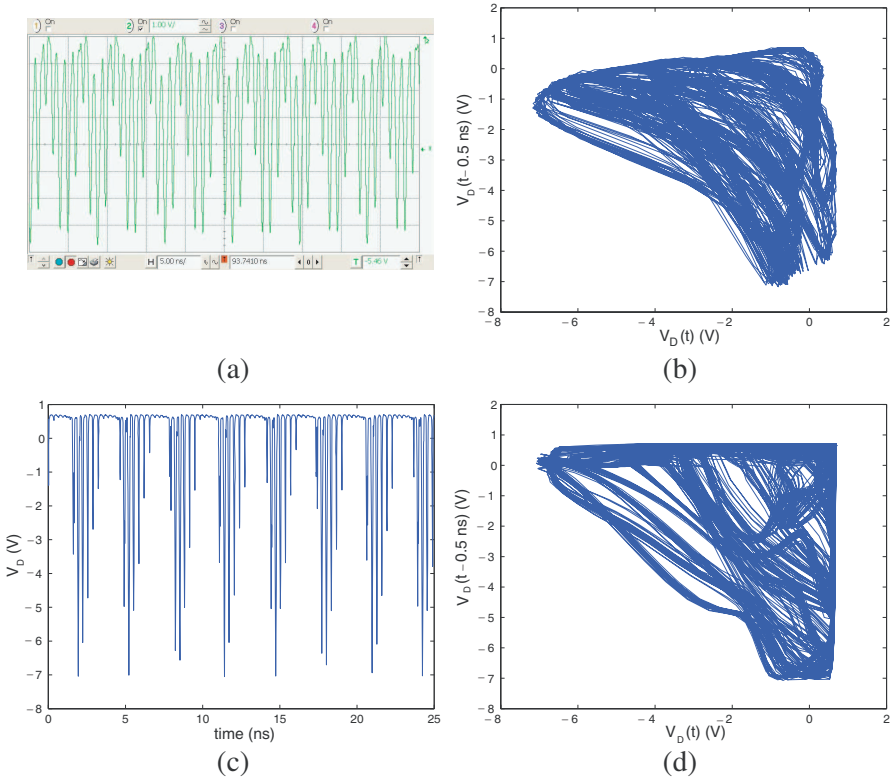

Figure 16. Theoretical and experimental chaotic behaviour for the loop antenna in the chaos conditions Table 1. (a) Screenshot showing the voltage $V_D\,(t)$, (b) experimental chaotic attractor, (c) theoretical voltage $V_D\,(t)$ using Matlab, (d) theoretical chaotic attractor using Matlab.

(Figure 10(b)). Under this condition, the real part of the radiation impedance is equal to zero, observed in Figures 4 and 10(a). However, this real part is different from zero value in the case of the experimental result Figure 10(b), due to the loss resistance of the experimental setup which is not included in the analytical equation.

To complete our chaos behaviour analysis, we are also interested in studying the attractors of each antenna in order to confirm the P_{drive} condition obtained from previous bifurcation diagrams.

As an example, for the patch antenna, the periodic behaviour is achieved at $P_{\text{drive}} = +24\,\text{dBm}$ (Figure 13) which corresponds to the periodic conditions obtained in the bifurcation diagrams.

For $P_{\text{drive}} = +29\,\text{dBm}$, the oscillation are chaotic, and attractor trajectory fills the phase space.

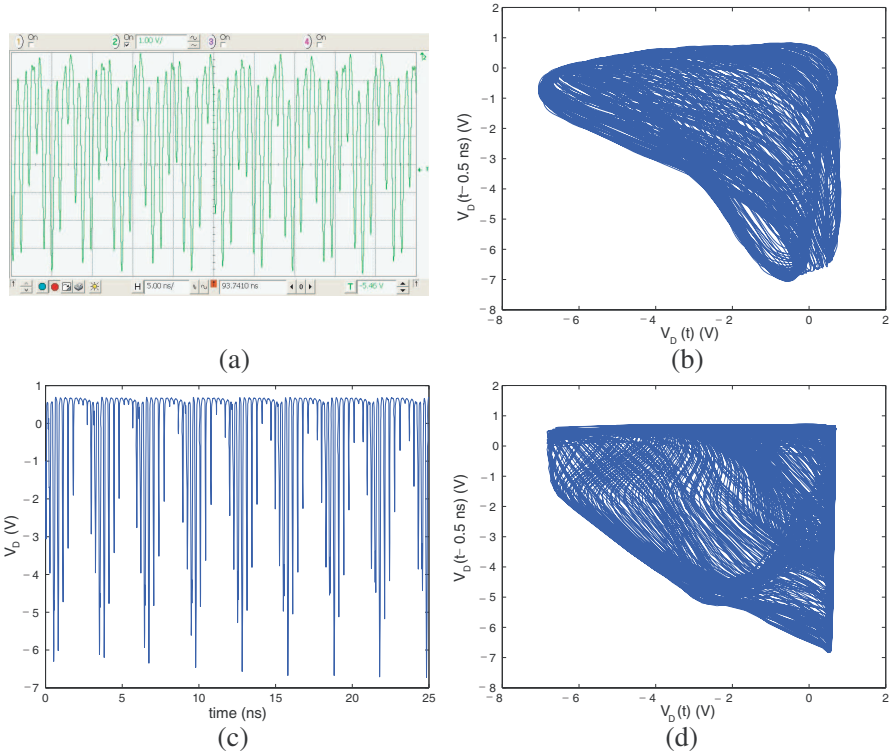

Figure 17. Theoretical and experimental chaotic behaviour for the horn antenna in the chaos conditions Table 1. (a) Screenshot showing the voltage $V_D\,(t)$, (b) experimental chaotic attractor, (c) theoretical voltage $V_D\,(t)$ using Matlab, (d) theoretical chaotic attractor using Matlab.

Table 1 summarizes the theoretical and experimental chaos conditions for each antenna.

Figures 14–17 depict the theoretical and experimental attractors respectively for patch, monopole, loop and horn antennas. These results demonstrate the chaotic behaviour of the studied antennas.

4. CONCLUSION

Experimental microwave chaos generation in a front-end receiver circuit has been demonstrated for several types of antennas. Bifurcation diagrams derived from a delay nonlinear differential equation have been presented for each antenna to predict the chaos conditions. Chaotic behaviour is confirmed by the attractor analysis. All the results show, for the first time, that when an electromagnetic interference signal is applied outside of the bandwidth of the antenna, chaos behaviour is created due to antenna mismatch combined with the nonlinearity of the front-end receiver circuit. On the other hand, this work is not restricted to the front-end receiver circuits, wireless applications or X-band applications. It could be expanded to other similar non linear circuit cases.

ACKNOWLEDGMENT

This work which concerns a PhD thesis is supported by the "DGA" ("Direction Générale de l'Armement") and the "CEA" ("Commissariat à l'Energie Atomique et aux Energies Alternatives").

REFERENCES

1. Glenn, C. M. and S. Hayes, "Observation of Chaos in a Microwave Limiter Circuit," *IEEE Microwave and Guided Wave Lett.*, Vol. 4, No. 12, 417–419, 1994.
2. Caroll, T. L. and L. M. Pecora, "Parameter ranges for the onset of period doubling in the diode resonator," *Phys. Rev. E*, Vol. 66, 2002.
3. Su, Z., R. W. Rollins, and E. R. Hunt, "Simulation and characterization of strange attractors in driven diode resonator systems," *Phys. Rev. A*, Vol. 40, 1989.
4. Tanaka, S., S. I. Higuchi, and T. Matsumoto, "Sheet structure in global bifurcations of a driven R-L-diode circuit," *Phys. Rev. E*, Vol. 54, 6014–6028, 1996.

5. Brorson, S. D., D. Dewey, and P. S. Linsay, "Self-replicating attractor of a driven semiconductor oscillator," *Phys. Rev. A*, Vol. 28, 1983.
6. Matsumoto, T., L. O. Chua, and S. Tanaka, "Simplest chaotic noautonomous circuit," *Phys. Rev. A*, Vol. 30, 1155–1157, 1984.
7. Granatstein, V. L., et al., "Effects of hight power microwaves and chaos in 21st century analog and digital electronics," *AFOSR, MURI*, Institute for Research in Electronics and Applied Physics, Univ. of Maryland College Park, MD 20743-3511, No. F496200110374, 2006.
8. Blakely, J. N., J. D. Holder, N. J. Corron, and S. D. Pethel, "Simply folded band chaos in a VHF microstrip oscillator," *Phys. Lett.*, Vol. 346, Nos. 1–3, 111–114, 2005.
9. Caudron, F., A. Ouslimani, R. Vézinet, and A.-E. Kasbari, "Chaotic behavior in receiver front-end limiters," *Progress In Electromagnetic Research Letters*, Vol. 23, 19–28, 2011.
10. Miligan, T. A., *Modern Antenna Design*, 2nd Edition, Wiley-Interscience, New Jersey, 2005.
11. Balanis, C. A., *Antenna Theory Analysis and Design*, Wiley-Interscience, New York, 2005.
12. Collin, R. E., *Field Theory of Guided Waves*, 2nd Edition, IEEE Press Series on Electromagnetic Wave Theory, Wiley, 1991.
13. Wheeler, H. A., "Transmission-line properties of a strip on a dielectric sheet on a plane," *IEEE Trans. on Microwave Theory and Techn.*, Vol. 25, No. 8, 631–647, 1977.
14. Manntel, "Wave and antenna training system," Man & Tel Co., Ltd., No. WATS-2002, Korea, 2008.